Eur. Phys. J. B **60**, 45–50 (2007)
DOI: 10.1140/epjb/e2007-00317-x

THE EUROPEAN PHYSICAL JOURNAL B

Electron transport in double-walled carbon nanotubes

T.S. Li[1,a], C.H. Lee[2], and M.F. Lin[2,b]

[1] Department of Electrical Engineering, Kun Shan University, Tainan, Taiwan, Republic of China
[2] Department of Physics, National Cheng Kung University, Tainan, Taiwan, Republic of China

Received 4 September 2007 / Received in final form 12 October 2007
Published online 23 November 2007 –

Abstract. The transport properties of finite length double-walled carbon nanotubes subject to the influences of a transverse electric field and a magnetic field with varying polar angles are investigated theoretically. The electrical conductance, thermal conductance and Peltier coefficient dependences on the external fields and symmetric configuration are studied in linear response regime. Prominent peak structures of the electrical conductance are predicted when varying the electric field strength. The features of the conductance peaks are found to be strongly dependent on the external fields and the intertube interactions. The heights of the electrical and thermal conductance peaks display the quantized behavior, while those of the Peltier coefficient do not. The conductance peaks are found to be broadened by the finite temperature.

PACS. 61.46.-w Nanoscale materials – 73.22.-f Electronic structure of nanoscale materials: clusters, nanoparticles, nanotubes, and nanocrystals – 85.35.Kt Nanotube devices

1 Introduction

There is tremendous interest in the transport properties of carbon nanotubes (CN's) [1] due to their potential use in novel nanodevices [2]. A hollow cylinder made up of a rolled-up graphite sheet is a single-walled carbon nanotube (SWCN), and multi-walled carbon nanotubes (MWCN's) are composed of several concentric hollow cylinders. The most noticeable feature of MWCN's is the existence of intertube interactions. Previous theoretical works have demonstrated that intertube interactions significantly alter the electronic and transport properties of hybrid nanotube systems, such as pseudogap opening in double-walled carbon nanotubes (DWCN's) [3,4], and diffusive transport in incommensurate MWCN's [5]. DWCN's are the simplest MWCN's, and they provide a good platform for studying the intertube interactions in MWCN's. Lately, it is feasible to synthesize highly purified SWCN's [6] and DWCN's [7] efficiently.

Electronic transport in low-dimensional systems has been extensively studied [8–12]. One of the most important results is that for a one-dimensional conductor, in the ballistic regime, the electrical conductance is quantized in multiples of the quantum $2e^2/h$ [8,9]. It has been speculated that similar behavior should exist for the thermal transport. Schwab and collaborators observed the quantum of the thermal conductance, $\kappa_o = \pi^2 k_B^2 T/3h$, in nanosized narrow wires [13]. Theoretical calculations show that a conducting SWCN has only two conducting channels, and predict that the electrical conductance will be $4e^2/h$ independent of radius and length [14,15]. Frank and collaborators found the quantized electrical conductance of MWCN's at room temperature [16]. The quantized conductance steps in solutions of MWCN's had also been reported by Urbina and co-workers [17]. The electrical conductance caused by intertube transfer was directly measured in telescoping MWCN's [18]. The experimentally observed linear T dependence of the thermal conductance at low-temperature may indicate the existence of quantized thermal conductance in SWCNs [19]. Theoretical calculations have shown that quasibound states cause electrical conductance oscillations in DWCN's [20]. In this work, the electrical and thermal transport properties of finite length DWCN's are investigated within the ballistic regime. Once the formulation for DWCN is established, the generalization to MWCN will be straight forward.

2 Theory

A finite length CN is formed by rolling a graphite sheet from the origin to the vector $\mathbf{C}_h = m\mathbf{a}_1 + n\mathbf{a}_2$, where $\mathbf{a}_1$ and $\mathbf{a}_2$ are the primitive lattice vectors of the graphene sheet. It has the radius $r = |\mathbf{C}_h|/2\pi = b\sqrt{3(m^2+mn+n^2)}/2\pi$ and the chiral angle $\xi = \tan^{-1}[-\sqrt{3}\,n/(2m+n)]$. $b = 1.42$ Å is the C–C bond length. The length of a finite CN is determined by the total number of carbon atoms (N_A). Therefore, a finite length CN can be characterized by $(m, n; N_A)$. With the periodic boundary condition imposing on the electron wave function along the circumference, the azimuthal wave vector

[a] e-mail: tsli@mail.ksu.edu.tw
[b] e-mail: mflin@mail.ncku.edu.tw

k_Φ equals J/r, and the angular momentum J is an integer. Details of the geometric and electronic structures of finite CNs are given in reference [21].

Transport properties of finite length DWCN's under a uniform transverse electric field and a magnetic field with arbitrary polar angle are investigated in this work. We employ the tight-binding model to calculate the electronic structures of CNs. In the presence of a uniform electric field F perpendicular to the nanotube axis, the onsite energy of the ith carbon atom in tight-binding calculations will be perturbed by the amount $\Delta E = -eFr\cos\Phi_i$, with Φ_i being the azimuthal angle between the electric field and the radial vector of the ith carbon atom. The nanotube axis and the electric field direction are assumed to be the z-axis and x-axis, respectively. The x-axis is chosen in a way that the nanotube is mirror symmetric about it. When a uniform magnetic field passes through a CN, the phase of the electron wave function, which is determined by the vector potential, will be modified. The magnetic field is assumed to have the polar angle α. Then the vector potential $\mathbf{A}$ equals $\phi_B\cos\alpha/2\pi r\hat{\Phi} + \phi_B\sin\alpha\sin\Phi/\pi r\hat{z}$, which will induce an extra phase factor $\exp(i2\pi\Delta G_{\mathbf{R}}/\phi_{B0})$ in the Hamiltonian matrix element between sites i and j. $\Delta G_{\mathbf{R}} = \int_{\mathbf{R}_i}^{\mathbf{R}_j}\mathbf{A}\cdot d\boldsymbol{l}$, $\phi_B = \pi r^2 B$, and $\phi_{B0} = hc/e$ is the magnetic flux quantum.

The (5, 5; 90)–(10, 10; 180) armchair DWCN with C_5 symmetry is chosen as a model study (Fig. 1a). The configuration of the inner tube is enlarged (the heavy curves), and projected onto the outer tube (the light curves). The intertube distance d^{io} is 3.39 Å, which is consistent with experimental measurements [1,22]. The nearest-neighbor tight-binding Hamiltonian is given as

$$H = \sum_{i,j} t_{i,j}^{in} c_i^+ c_j + W\sum_{k,l} t_{k,l}^{io} e^{(d^{io}-d_{kl})/\delta} c_k^+ c_l\,, \qquad (1)$$

where $t_{i,j}^{in}$ and $t_{k,l}^{io}$ are the intratube and intertube transfer integrals, respectively. Only hopping between the nearest neighbors are considered. The intertube interactions are assumed to decay exponentially with interatom distance d_{kl}, as given in equation (1). $\delta = 0.45$ Å and the parameter W is chosen to be 1/16. The details of assigning the Hamiltonian matrix elements are given in references [23,24]. c_i^+ and c_j are the creation and annihilation operators at sites i and j, respectively.

After diagonalizing the Hamiltonian, the state energy $E^{c,v}(F,\phi_B,\alpha)$ can be obtained. The superscripts c and v, represent the antibonding π^* state and the bonding π state, respectively. With the inclusion of the Zeeman effect, the total state energy becomes $E^{c,v}(F,\phi_B,\alpha;\sigma) = E^{c,v}(F,\phi_B,\alpha) + g\sigma\phi_B/(m^* r^2\phi_{B0})$. The g factor is designated to be the same as that ($\sim$2) of graphite, where $\sigma = \pm 1/2$ is the electron spin and m^* is the bare electron mass.

We consider a finite length DWCN in a transverse electric field and a magnetic field with polar angle α, which is suspended between two reservoirs (macroscopic leads). The left and right reservoirs are assumed to have the chemical potentials and the temperatures $(\mu + eV,\ T)$ and $(\mu,\ T+\Delta T)$, respectively. In the ballistic regime, making use of the Landauer-Buttiker formula, the net electric and thermal currents are, respectively, given by

$$I(F,\phi_B,\alpha) = \frac{e}{h}\int dE\, T(E,F,\phi_B,\alpha) \times\left[f^o\left(\frac{E-\mu-eV}{T}\right) - f^o\left(\frac{E-\mu}{T+\Delta T}\right)\right] \qquad (2)$$

and

$$U(F,\phi_B,\alpha) = \frac{1}{h}\int dE\,(E-\mu)T(E,F,\phi_B,\alpha) \times\left[f^o\left(\frac{E-\mu-eV}{T}\right) - f^o\left(\frac{E-\mu}{T+\Delta T}\right)\right], \qquad (3)$$

where f^o is the Fermi-Dirac distribution function, and the elastic transmission coefficient is approximately given as

$$T(E,F,\phi_B,\alpha) = 2T_{res}\sum_{c,v,\sigma}\frac{\Gamma^2}{[E^{c,v}(F,\phi_B,\alpha;\sigma)-E]^2+\Gamma^2}, \qquad (4)$$

where Γ is the broadening width of the electron state energy caused by leaking into the emitter or collector. In this study, Γ is chosen to be $3.3\times10^{-5}\gamma_o$ ($\sim$ 0.1 meV; γ_o = 2.66 eV). T_{res} is the transmission probability at resonance ($E^c(F,\phi_B,\alpha;\sigma) = E$).

Within the linear-response approximation ($\Delta T \to 0$ and $V \to 0$), I is reduced to $\mathcal{L}_0 V - (\mathcal{L}_1\Delta T/T)$ and U

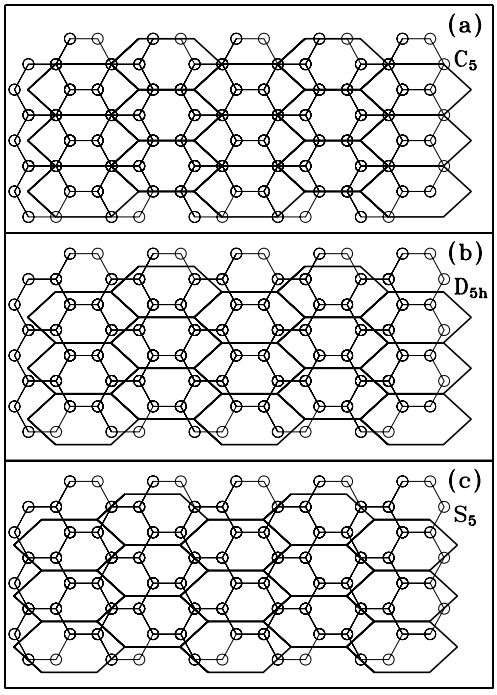

Fig. 1. Three kinds of symmetric configurations of the (5, 5; 90)–(10, 10; 180) DWCN are shown: (a) C_5, (b) D_{5h}, and (c) S_5. The inner tube is enlarged (the heavy curves), and projected onto the outer tube (the light curves).

becomes $\mathcal{L}_1 V - (\mathcal{L}_2 \Delta T/T)$. The electrical conductance is defined by $G = I/V = \mathcal{L}_0$ at $\Delta T = 0$. The Peltier coefficient Π, which is related to the electromotive force (E.M.F.) generated by the system in response to a temperature gradient when $I = 0$, is $\mathcal{L}_1/\mathcal{L}_0$. The thermal conductance κ, defined as the net thermal current produced by a temperature gradient at $I = 0$, is given by $(\mathcal{L}_2 - \mathcal{L}_1^2 \mathcal{L}_0^{-1})/T$. $\mathcal{L}_\beta(F)$ is defined as

$$\mathcal{L}_\beta(F) = \frac{e^{2-\beta}}{h} \int dE\, (E-\mu)^\beta \times T(E, F, \phi_B, \alpha) \frac{-\partial f^o(E)}{\partial E}. \quad (5)$$

At low temperatures, the main contributions to $\mathcal{L}_\beta$ ($\beta = 1, 2, 3$) come from electronic states very close to the chemical potential.

3 Results and discussion

The (5, 5; 90)–(10, 10; 180) armchair DWCN with C_5 symmetry has been chosen as a model study. State energies without intertube interactions (independent tubes) are shown in Figure 2a. Electronic energies are symmetric about the Fermi level. The intertube interactions will reduce the energy gap, change the curvature or the F dependence of the state energy, and the electronic structures are no longer symmetric about the Fermi level (Fig. 2b). A parallel magnetic field ($\alpha = 0°$) will modify the curvature (Fig. 2c), but a transverse magnetic field ($\alpha = 90°$; Fig. 2d) will not. That the parallel magnetic field would induce a shift in k_Φ from J/r to $(J + \cos\alpha\, \phi_B/\phi_{B0})/r$ is the main reason. The Zeeman splitting would introduce a further split for the spin-up and spin-down states. The changes in state energies at $\alpha = 90°$ are mainly caused by the Zeeman effect (Fig. 2d).

The electrical conductance displays sharp peak structures with varying F (Fig. 3). Explanations of the spike behavior are as follows. The $\partial f(E)/\partial E$ function is a prominent Lorentzian function at the Fermi energy. The electron state energies rely sensitively on F [25–28]. Therefore, the lowest state may touch the Fermi level and contributes to the electrical conductance, or untouch the Fermi level and does not contribute as F differs slightly. The positions of the peak correspond to the F values that lead to the semiconductor-metal transitions, and their heights are related to the number of states at the Fermi level. Considering the cases with $\phi_B = 0$, when there is no intertube interaction, there are two peaks. The intertube interactions will alter the positions of the peaks depending on the symmetric configuration (Figs. 3b–3d). The heights of the peaks display quantized behavior. The inclusion of magnetic field will generally halve the heights (Figs. 3a–3d). It can be explained as follow. The peak is contributed equally by the spin-up and spin-down states, when $\phi_B = 0$. An external magnetic field will break the spin degeneracy and shift the state energies. The resulting states might or might not cross the Fermi level. If they do cross the Fermi level, their heights will be half of the original values. We have also calculated the electrical conductance of C_5 system for different α (Figs. 3b, 3e–3g). The ballistic transport properties are found to essentially rely on how the states cross the Fermi energy as the external fields vary. The difference in α only affects when and where the crossing occurs. It only modifies the number and positions of the peaks. Moreover, the effects of the magnetic field are less manifested at large F. The double peaks' structures around $F = 0.08\ \gamma_o/e$ Å depend weakly on α (Figs. 3b, 3e–3g).

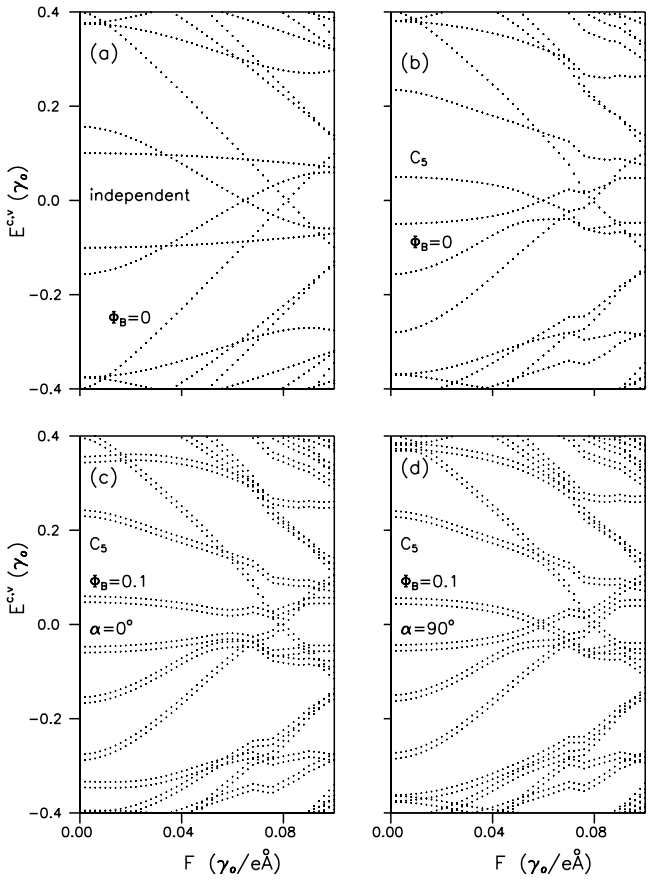

Fig. 2. The state energies versus the transverse electric field strength F for the (5, 5; 90)–(10, 10; 180) DWCN with (a) no intertube interaction and $\phi_B = 0$, (b) C_5 symmetry and $\phi_B = 0$, (c) C_5 symmetry, $\phi_B = 0.1\phi_{B0}$ and $\alpha = 0°$; (d) C_5 symmetry, $\phi_B = 0.1\phi_{B0}$ and $\alpha = 90°$. The Fermi level equals zero.

Comparing Figures 3 and 4, it is obvious that the number, heights, and positions of the thermal conductance peaks are closely corresponding to those of the electrical conductance (Figs. 4a–4d). The Wiedemann-Franz (WF) law, as discussed later in equation (6), is the main reason. On the other hand, there are differences in the shape and extent of the peaks between the electrical conductance and thermal conductance. The differences are originated from the different integrand in equation (5). The computed Peltier coefficient exhibits antisymmetric structures with peaks and dips (Figs. 4e–4h). It is caused by

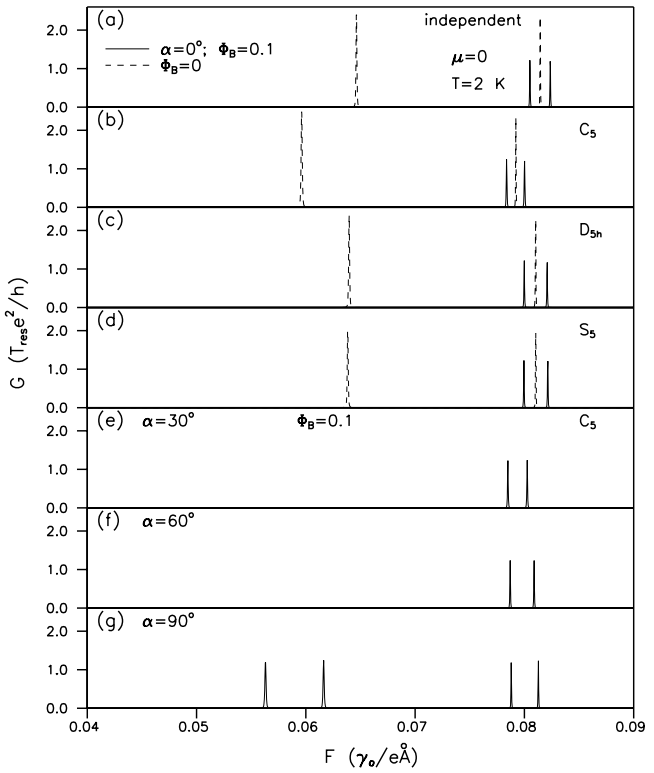

Fig. 3. The electric-field-dependent electrical conductance at $T = 2$ K, $\mu = 0$, $\phi_B = 0.1\ \phi_{B0}$, and $\alpha = 0°$ for the (5, 5; 90)–(10, 10; 180) DWCN for four kinds of intertube interactions: (a) no intertube interaction, (b) C_5, (c) D_{5h}, and (d) S_5. The cases with $\phi_B = 0$ are shown as dashed line. Electrical conductance dependence on the electric field strength F for the C_5 projection at $\phi_B = 0.1\phi_{B0}$ with (e) $\alpha = 30°$, (f) $\alpha = 60°$, and (g) $\alpha = 90°$.

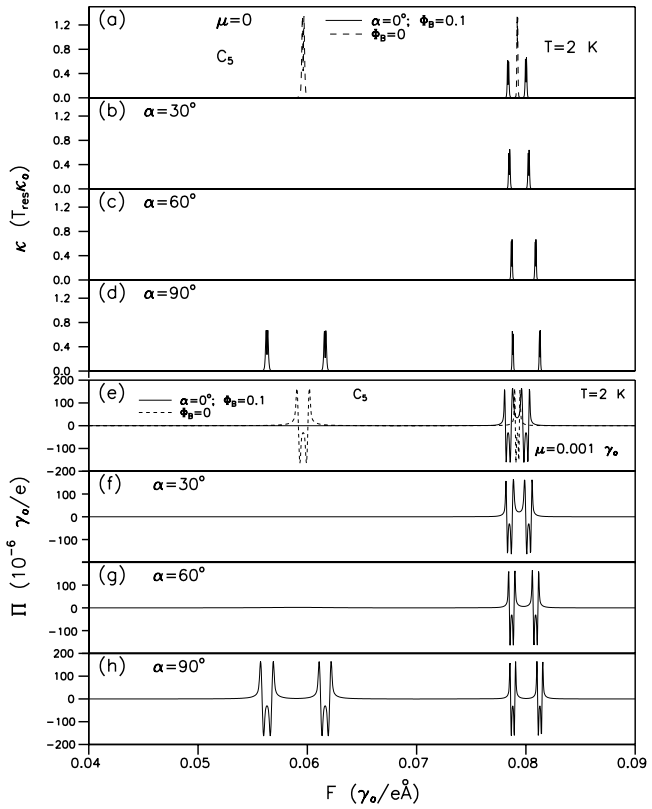

Fig. 4. The electric-field-dependent thermal conductance at $T = 2$ K, $\mu = 0$, and $\phi_B = 0.1\ \phi_{B0}$ for the (5, 5; 90)–(10, 10; 180) DWCN with C_5 symmetry at (a) $\alpha = 0°$, (b) $\alpha = 30°$, (c) $\alpha = 60°$, and (d) $\alpha = 90°$. The electric-field-dependent Peltier coefficient at $\mu = 0.001\gamma_o$, $\phi_B = 0.1\phi_{B0}$ with (e) $\alpha = 0°$, (f) $\alpha = 30°$, (g) $\alpha = 60°$, and (h) $\alpha = 90°$. The cases with $\phi_B = 0$ are shown as dashed line.

the antisymmetry of the integrand of $\mathcal{L}_1$. Moreover, the heights of Π do not exhibit the quantized behavior, and they are independent of the spin degeneracy. The functions $\mathcal{L}_0$ and $\mathcal{L}_1$ are individually proportional to the number of degenerate states at μ, but the ratio or Π is not.

The thermal broadening effects on the conductance peaks are demonstrated in Figures 5a–5b. The $\partial f(E)/\partial E$ prominent Lorentzian function is widened by the finite temperature with a width k_BT, and consequently the number of conducting states is also altered. The pronounced peak structure of the electrical conductance and the thermal conductance are gradually stretched by the increasing temperature. At the same temperature, the integrand of $\mathcal{L}_2$ (Eq. (5)), which is quadratic in $E - \mu$, is more extended in energy domain than that of $\mathcal{L}_0$. Therefore, κ is more susceptible to the thermal broadening effect than G.

At small T, $\mathcal{L}_2$ can be approximated as $\mathcal{L}_2 \approx \pi^2 k_B^2 T^2 \mathcal{L}_0/3e^2$. For a SWCN, as pointed out by Lin and coworkers [29], $\mathcal{L}_2 \gg \mathcal{L}_1^2\mathcal{L}_0^{-1}$, thus

$$\kappa \approx \frac{\mathcal{L}_2}{T} \approx \frac{\pi^2 k_B^2 T}{3e^2} G, \tag{6}$$

which is the Wiedemann-Franz law. It is of interest to investigate whether this law holds for finite length DWCN's. Caused by the different sensitivity on temperature between κ and G, the ratio κ/G fluctuates strongly about 1 (in unit of $\pi^2 k_B^2 T/3e^2$) when states get close to μ (Fig. 6). The amplitude of fluctuation increases with temperature. However, the WF law is well obeyed in a wide range of F when the states depart from μ. Depolarization or screening effects, which arise from redistribution of carriers induced by the external electric field, have not been taken in account. A thorough investigation of the effective electric field would require the self-consistent field approach [30–32]. In this study, F is the effective electric field strength, and the external (or applied) electric field strength is roughly determined to be five times of F in a carbon nanotube, according to calculations given in literatures [28, 32,33]. Quantitative estimate of the field intensity is beneficial for readers performing experimental study. The magnetic field strength corresponding to $\phi_B = 0.1\phi_{B0}$ is 286.3 T, and $F = 0.1\gamma_o/e$ Å is 0.266 $V/$ Å. The armchair DWCN's considered in this study are commensurate systems with well-defined unit cell, and the Bloch theorem is applicable. In general, incommensurate DWCN's do not have rotational symmetries, and the Bloch theorem

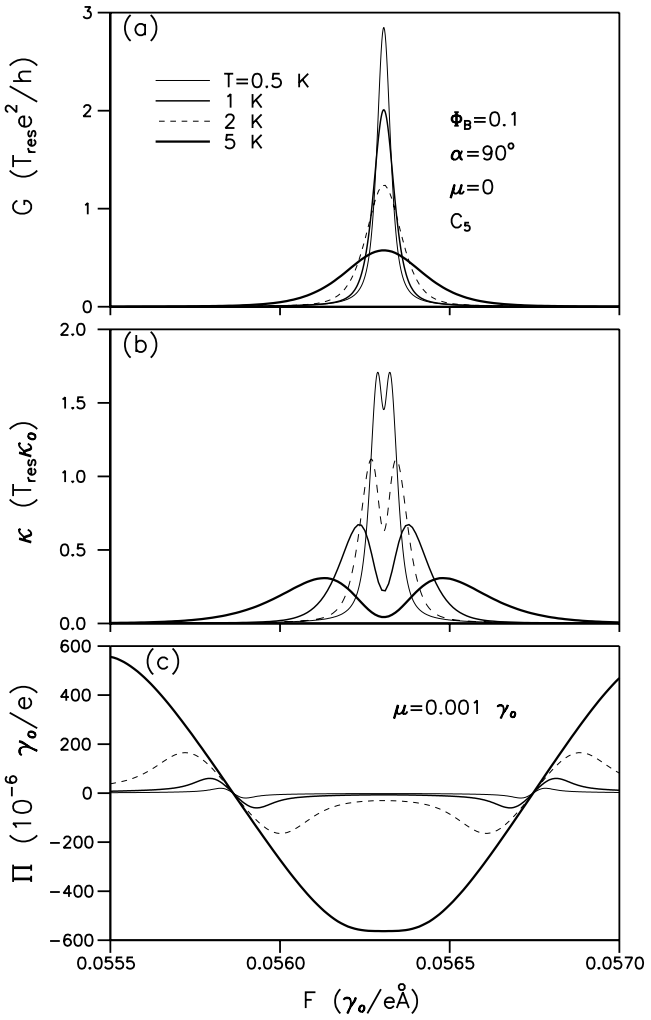

Fig. 5. The dependence of (a) the electrical conductance, (b) the thermal conductance, and (c) the Peltier coefficient on the electric field strength F at $\phi_B = 0.1\phi_{B0}$ and $\alpha = 90^\circ$ for the (5, 5; 90)–(10, 10; 180) DWCN with C_5 symmetry at various temperatures.

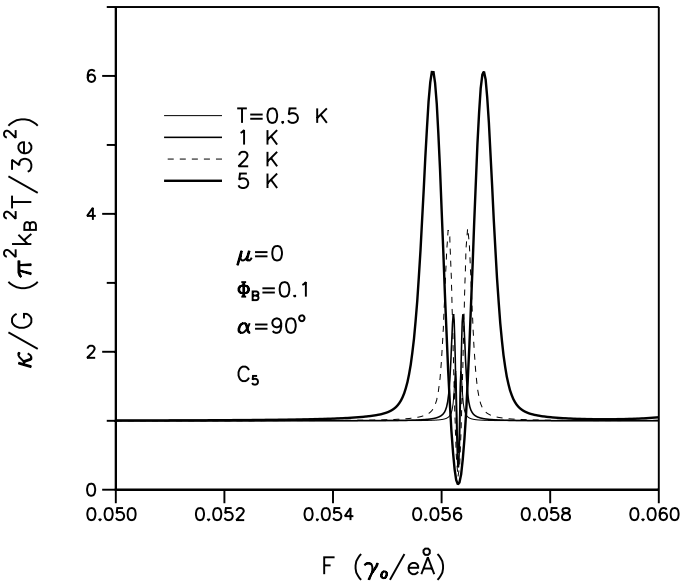

Fig. 6. Relation between the thermal conductance and the electrical conductance versus F for the (5, 5; 90)–(10, 10; 180) DWCN with C_5 symmetry at $\phi_B = 0.1\phi_{B0}$, $\alpha = 90^\circ$, and $\mu = 0$ with various temperatures.

is no longer applicable. Therefore, our approach cannot be used for incommensurate systems. The electronic properties of incommensurate carbon nanotube systems are documented in reference [34]. In this work, the nanotubes are assumed to be defect-free. Chico and co-workers investigates the quantum conductance of SWCN's with defects by the Green's function matching method [35]. They found that a single vacancy produces a dramatic decrease in the conductance of small-radius tubes. Son and collaborators studied the resistance of defective metallic SWCN in a transverse electric field by first-principles calculations [36], and demonstrated that the resistance is tunable up to three orders of magnitude by both defects and electric field.

4 Concluding remarks

In conclusion, the transport properties of finite length double-walled carbon nanotubes subject to the influences of a transverse electric field and a magnetic field with varying polar angles are investigated theoretically. The electrical conductance, thermal conductance and Peltier coefficient dependence on the external fields and symmetric configuration is studied in linear response regime. Prominent peak structures of the electrical conductance are predicted when varying the electric field strength. The number, heights, and positions of the conductance peaks are found to be strongly dependent on the external fields and the intertube interactions. The heights of the electrical and thermal conductance peaks display the quantized behavior, while those of the Peltier coefficient do not. The conductance peaks are broadened by the finite temperature. Moreover, it is found that the validity of the Wiedemann-Franz law relies upon the temperature, the field strength, the electronic structure, and the chemical potential. This formulation can be generalized and applied to MWCN.

This work was supported in part by the National Science Council of Taiwan, the Republic of China under Grant No. NSC 95-2221-E-168-038.

References

1. S. Iijima, Nature **354**, 56 (1991)
2. S.J. Tans, M.H. Devoret, H. Dai, A. Thess, R.E. Smalley, L.J. Geerligs, C. Dekker, Nature **386**, 474 (1997)
3. K.Y. Kwon, D. Tománek, Phys. Rev. B **58**, R16001 (1998)
4. S. Sanvito, K.Y. Kwon, D. Tománek, C.J. Lambert, Phys. Rev. Lett. **84**, 1974 (2000)
5. S. Roche, F. Triozon, A. Rubio, D. Mayou, Phys. Lett. A **285**, 94 (2001)

6. K. Hata, D.N. Futaba, K. Mizuno, T. Namai, M. Yumura, S. Iijima, Science **306**, 1362 (2004)
7. M. Endo, H. Muramatsu, T. Hayashi, Y.A. Kim, M. Terrones, M.S. Dresselhaus, Nature **433**, 476 (2005)
8. R. Landauer, IBM J. Res. Dev. **1**, 223 (1957)
9. R. Landauer, Philos. Mag. **21**, 863 (1970)
10. B.J. van Wees, H. van Houten, C.W.J. Beenakker, J.G. Williamson, L.P. Kouwenhoven, D. van der Marel, C.T. Foxon, Phys. Rev. Lett. **60**, 848 (1988)
11. W.J. Skocpol, P.M. Mankiewwich, R.E. Howard, L.D. Jackel, D.M. Tennant, A.D. Stone, Phys. Rev. Lett. **56**, 2865 (1986)
12. S. Datta, *Electronic Transport in Mesoscopic Systems* (Cambridge University Press, Cambridge, England, 1995)
13. K. Schwab, E.A. Henriksen, J.M. Worlock, M.L. Roukes, Nature **404**, 974 (2000)
14. M.F. Lin, K.W.K. Shung, Phys. Rev. B **51**, 7592 (1995)
15. L. Chico, L.X. Benedict, S.G. Louie, M.L. Cohen, Phys. Rev. B **54**, 2600 (1996)
16. S. Frank, P. Poncharal, Z.L. Wang, W.A. de Heer, Science **280**, 1744 (1998)
17. A. Urbina, I. Echeverria, J. Abellan, Phys. Rev. Lett. **90**, 106603 (2003)
18. J. Cumings, A. Zettl, Phys. Rev. Lett. **93**, 086801 (2004)
19. J. Hone, M. Whitney, C. Piskoti, A. Zettl, Phys. Rev. B **59**, R2514 (1999)
20. D.H. Kim, K.J. Chang, Phys. Rev. B **66**, 155402 (2002)
21. R.B. Chen, C.P. Chang, J.S. Hwang, D.S. Chuu, M.F. Lin, J. Phys. Soc. Jpn **74**, 1404 (2005)
22. J. Wei, B. Jiang, X. Zhang, H. Zhu, D. Wu, Chem. Phys. Lett. **376**, 753 (2003)
23. Y.H. Ho, C.P. Chang, F.L. Shyu, R.B. Chen, S.C. Chen, M.F. Lin, Carbon **42**, 3159 (2004)
24. G.W. Ho, Y.H. Ho, T.S. Li, C.P. Chang, M.F. Lin, Carbon **44**, 2323 (2006)
25. X. Zhou, H. Chen, O.Y. Zhang-can, J. Phys.: Condens. Matter **13**, L635 (2001)
26. D.H. Kim, K.J. Chang, Phys. Rev. B **64**, 153404 (2001)
27. T.S. Li, M.F. Lin, Phys. Rev. B **73**, 075432 (2006)
28. Y. Li, V. Rotkin, U. Ravaioli, Nano Lett. **3**, 183 (2003)
29. M.F. Lin, D.S. Chuu, K.W.K. Shung, Phys. Rev. B **53**, 11186 (1996)
30. H. Ehrenreich, M.H. Cohen, Phys. Rev. **115**, 786 (1959)
31. T.S. Li, M.F. Lin, J. Phys. Soc. Jpn **74**, 425 (2005)
32. S.C. Chen, W.C. Hseih, M.F. Lin, Phys. Rev. B **72**, 193412 (2005)
33. L.X. Benedict, S.G. Louie, M.L. Cohen, Phys. Rev. B **52**, 8541 (1995)
34. J.C. Chairler, X. Blase, S. Roche, Rev. Mod. Phys. **79**, 677 (2007)
35. L. Chico, L.X. Benedict, S.G. Louie, M.L. Cohen, Phys. Rev. B **54**, 2600 (1996)
36. Y.W. Son, J. Ihm, M.L. Cohen, S.G. Louie, H.J. Choi Phys. Rev. Lett. **95**, 216602 (2005)